R-04-28

Deep penetrating eddy current for copper canister inspection

Main results

Tadeusz Stepinski, TSonic

February 2004

Svensk Kärnbränslehantering AB
Swedish Nuclear Fuel
and Waste Management Co
Box 5864
SE-102 40 Stockholm Sweden
Tel 08-459 84 00
+46 8 459 84 00
Fax 08-661 57 19
+46 8 661 57 19

ISSN 1402-3091
SKB Rapport R-04-28

Deep penetrating eddy current for copper canister inspection

Main results

Tadeusz Stepinski, TSonic

February 2004

Contents

1 Introduction 5

2 Experimental setup 7

3 Processing EC signals 11
3.1 Magnitude estimation 11
3.2 SNR estimation 12
3.3 Automatic phase estimation 13
3.4 Distortion free signal filtering 14

4 Results 17
4.1 Probe comparison 17
4.1.1 Rohman probe 17
4.1.2 Leotest probes 18
4.2 Detection limits 20
4.3 Circular voids 21
4.4 Rectangular voids 22
4.4.1 Phase angles 22
4.4.2 Defect size 23
4.5 Comparison of EC indications for rectangular and circular defects 25
4.5.1 Phase angles 25
4.5.2 Defect size estimation 26
4.5.3 Shapes of the EC patterns 28

5 Comparison of copper material 31
5.1 Phase angles 32
5.2 Response magnitudes 33

6 Conclusions 36

7 References 37

Appendix 1 39
Appendix 2 41
Appendix 3 43

1 Introduction

The aim of this project was to optimize the detection and characterization of deep flaws (voids) in copper plates. Two types of voids were investigated and compared: circular and rectangular. The circular voids had the form of cylindrical cavities while the rectangular ones were cavities with a rectangular cross section. The following EC probes have been tested in the experiments:

Manufacturer	EC Probe	Approx diameter of active zone	Test performed by
ESR Rohman	MDK 33	18 mm	TSonic
LEOTEST-Lvov	MDF 12	12 mm	TSonic
LEOTEST-Lvov	MDF 08	8 mm	TSonic

All probes were of the same type, transmit- receive transducers with four pick-ups connected in a double differential configuration. The ESR probe is a standard deep-penetrating EC transducer used mostly for inspection of aluminum sandwich structures. The MDF probes are low frequency multi-differential probes that were specially manufactured for this project by LEOTEST in Lvov. The detection ability of the above probes was evaluated using specially designed sandwich specimens presented below.

Detailed results acquired with each probe were presented in former reports /1/, /2/. Here, we present only the results obtained with the MDF 12 since it appeared to have the best performance in our application. The relation between eddy current responses and the defect parameters (defect depth and size) established for this probe is also presented. This relation was used for the development of the defect characterization method.

2 Experimental setup

ESR Rohman PL.E EC instrument with the following settings was used in the experiments:

Operating frequency	720 Hz
Probe excitation	50 Ω
Phase	0°
Gain	60–85 dB (depending on upper plate thickness)
Filter	DC to 8 Hz

Special test specimens were manufactured to simulate voids in copper of different shapes and volumes located at different depths. The specimens had the form of a sandwich consisting of three layers: the upper one for simulating given depth, the middle one with holes, and the bottom plate (cf Figure 2-1). To assure minimum gaps between the plates a special system of air channels was manufactured in the upper and base plate that enabled pumping out air from the space between the plates using a vacuum pump. Then the atmospheric pressure pressed the plates together (see Appendix 3 for details).

Void depth, t_d could be varied by changing the thickness of the upper plate. Void volume was a function of thickness of the middle plate t_v and void cross section. Two types of middle plates were used: the plates with drilled holes of different diameters, and the plates with rectangular windows manufactured using EDM (see Appendix 1 for details).

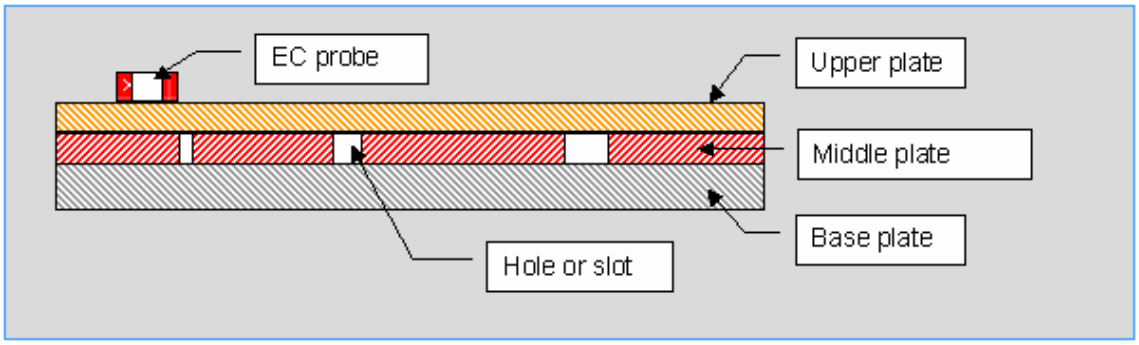

Figure 2-1. *Test object simulating voids with certain form and volume located at certain depth.*

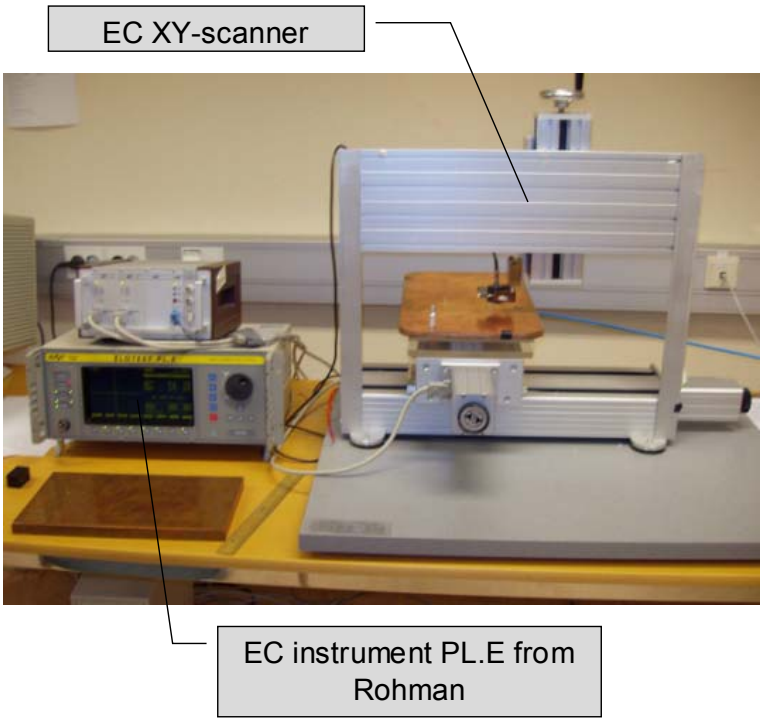

Figure 2-2. *Test setup used in experiments.*

A series of measurements was performed to evaluate and compare the performance of the MDF12 probe on holes and rectangular voids. The measurements were performed using the XY scanner shown in Figure 2-2. The scanner was controlled by a PC, which acquired data from two analog outputs of the EC instrument.

Linear scans of the voids with different cross sections, placed under upper plates with depths t_d from 1 mm to 3 mm, were performed. The voids had different volumes due to the variable thickness t_h of the middle plate (cf Figure 2-1). Dimensions of the holes and the rectangular voids used in test are listed in Tables 2-1 and 2-2.

Table 2-1. Hole areas depending on hole diameter (in mm^2).

Hole diameter (mm)	Hole cross section (mm^2)
0.8	0.5
1.0	0.8
1.2	1.1
1.5	1.8
1.8	2.5

Table 2-2. Rectangular voids and their cross sections (in mm^2).

Defect width (mm)	Cross section (mm^2)		
	Defect length 1 mm	Defect length 2 mm	Defect length 3 mm
0.3 mm	0.3	0.6	0.9
0.6 mm	0.6	1.2	1.8

Sensitivity of the MDF probe to the void shape was compared in the experiments using two equivalence criteria: cross section area and lengths/diameter. Table 2-3 presents diameters of the circular voids that were used for the comparison to the rectangular voids using cross section as a criterion.

Table 2-3. Rectangular voids and holes used for the comparison.

Rectangular defect cross section (mm^2)	Hole cross section (mm^2)	Hole diameter (mm)
0.3	0.5	0.8
0.6	0.8	1.0
0.9	1.1	1.2
1.2	1.1	1.2
1.8	1.8	1.5

The probe was scanned in contact with the upper plate using the XY scanner and the EC data was stored in the PC. Due to the specimen geometry and scanner size only three holes could be scanned at a time and therefore the results obtained for separate scans for each combination of the upper and middle plates are slightly different.

3 Processing EC signals

The EC data acquired in different scans was normalized with respect to the instrument gain and filtered by a digital linear phase filter that removed noise without changing signal shape. Finally, magnitude and phase of the individual EC signals was estimated.

3.1 Magnitude estimation

Signal magnitude A_{max} was found as the maximum length of the signal projection on the direction defined by its phase (difference between the maximum and minimum amplitude). This is illustrated by the signal example shown in Figure 3-1.

The second measure of signal magnitude, A_{std} was the standard deviation of the signal magnitude calculated using the following formulas:

$$A_{std} = \frac{1}{N-1}\sqrt{\sum_N (|s_i| - \bar{s})^2} \quad where \quad \bar{s} = \frac{1}{N}\sum_N |s_i| \tag{1}$$

where $\{s_1, s_2, \ldots s_i, \ldots s_N\}$ represents a set of N complex valued samples of the EC signal that form the whole EC response.

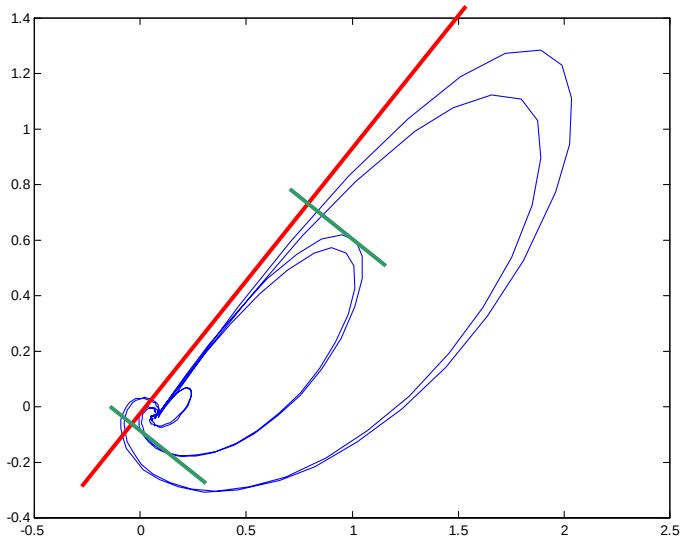

Figure 3-1. *Example responses of the MDF Probe for 3 different holes. Red line defines signal phase and interval between the green lines is a measure of signal amplitude.*

3.2 SNR estimation

Signal to noise ratio (SNR) was required to establish the detection limit (the deepest void that can be reliably detected). Signal to noise ratios were calculated using the following formulas:

$$S/N_{std} = 20\log\left(\frac{\sigma_{signal}}{\sigma_{noise}}\right) \qquad S/N_{abs} = 20\log\left(\frac{\Delta_{signal}}{\Delta_{noise}}\right) \tag{2}$$

where

σ_{signal}, σ_{noise} – standard deviations of signal and noise, respectively
Δ_{signal}, Δ_{noise} – max variation of signal and noise, respectively

Figure 3-2 shows intervals where the above-mentioned signal and noise parameters were measured.

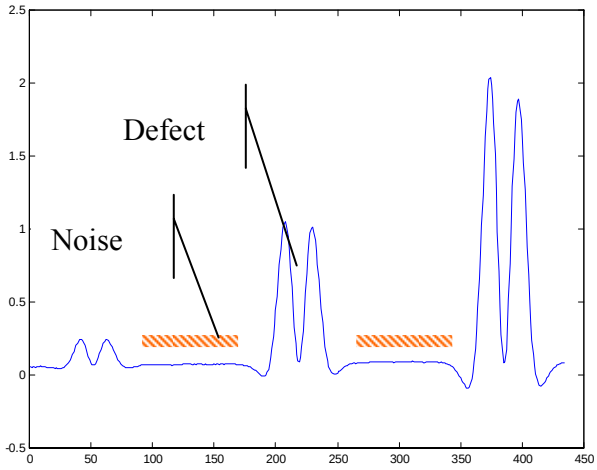

Figure 3-2. *In-phase component of the signal from Figure 3-1. Red dashed lines define intervals used for calculating noise levels.*

3.3 Automatic phase estimation

The method used for the evaluation of EC data uses the information contained in second order central moments of the contour formed by the probe response in the impedance plane, /5/. The second order central moments for the in-phase and quadrature components of the complex valued continuous EC signal $s(t) = g[x(t), y(t)] = P(t) + jQ(t)$ can be defined as

$$\mu_{20} = \int_{-\infty}^{\infty}\int_{-\infty}^{\infty}(x-\mu_x)^2 g(x,y)dxdy; \quad \mu_{02} = \int_{-\infty}^{\infty}\int_{-\infty}^{\infty}(y-\mu_y)^2 g(x,y)dxdy \tag{3}$$

$$\mu_{11} = \int_{-\infty}^{\infty}\int_{-\infty}^{\infty}(x-\mu_x)(y-\mu_y)g(x,y)dxdy$$

where t denotes scanning coordinate (length or time) μ_x, μ_y are the respective mean values of the function $g(x,y)$, and $x(t)$, $y(t)$ are the respective real and imaginary parts of the signal $s(t)$ in the impedance plane.

Let us calculate the covariance matrix **V**, which includes second order central moments

$$\mathbf{V} = \begin{bmatrix} \mu_{20} & \mu_{11} \\ \mu_{11} & \mu_{02} \end{bmatrix} \tag{4}$$

This matrix has two eigenvectors pointing at the main directions of the pattern. The eigenvector corresponding to the larger eigenvalue indicates phase of the EC pattern. The other eigenvector that is orthogonal to the first one indicates pattern's width.

Three EC responses to 3 rectangular voids are shown in Figure 3-3 together with the estimated phase angles. The solid lines in Figure 3-3 show directions of the respective eigenvectors calculated for the 3 patterns shown in this figure. Since all voids are at the same depth their phase angles are identical.

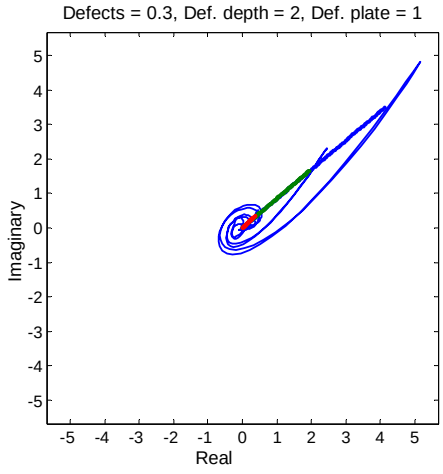

Figure 3-3. *Automatic phase angle estimation for responses of rectangular voids at 2 mm depth.*

The covariance matrix for the signals presented in this report was calculated for the pattern discretized using equidistant sampling of the in-phase and quadrature components with respect to the scanning coordinate *t*. Thus after the discretization the pattern is defined as

$$P(t_n) + jQ(t_n) = g(x_n, y_n) = g(n) \tag{5}$$

where $t_n = t_{n-1} + \Delta t$ is the discretized scanning coordinate (distance along the voids).

Since the EC signals, especially those acquired from deep located voids were quite noisy the discretized patterns were filtered before applying the phase estimation method presented above.

3.4 Distortion free signal filtering

Classical filters used for the filtering in-phase and quadrature components of the EC signals introduce a serious distortion of the EC patterns that depends on the filter parameters. This is due to the nonlinear phase response of infinite impulse response (IIR) filters that results in different phase delays of the individual frequency components of the EC signals. This distortion can be avoided by using linear phase filters for filtering EC signals, see /3/. The linear phase filters can take different forms depending on the application.

Here, we propose a simple filtering scheme in frequency domain based on the FFT of the sampled EC signals. The desired filtering operation can be achieved by zeroing the undesired frequencies in the discrete spectrum of the EC signal and subsequent inverse FFT operation of the trimmed spectrum.

Generally, filtering of a high frequency electronic noise results in only a few lowest frequencies are left in the spectrum. If we assume that the discrete EC signal, Equation (5) is periodic with period *N,* then we can express it using a finite number of Fourier coefficients

$$\begin{aligned} g(n) &= \sum_{k=0}^{N-1} a_k e^{jk(2\pi/N)n} \cong \sum_{l=1}^{L} a_l e^{jl(2\pi/N)n} \quad \textit{where} \quad L \le N \\ a_k &= \frac{1}{N}\sum_{n=0}^{N-1} g(n) e^{-jk(2\pi/N)n} \qquad a_l = \frac{1}{N}\sum_{n=0}^{N-1} g(n) e^{-jl(2\pi/N)n} \end{aligned} \tag{6}$$

where a_k , a_l denote complex valued coefficients in the Fourier expansion of the contour *g(n)*. In general case the Fourier spectrum of a complex valued signal is nonsymmetric and *L* coefficients in its expansion are needed to define *L/2* lowest frequencies. Therefore, the indices *k* and *l* in Equation (6) are not equal ($k \neq l$).

In most cases only few coefficients are sufficient for preserving the shape of the EC pattern. An example illustrating this type of filtering is demonstrated in Figure 3-3 where two typical scans for a hole (Figure 3-4a) and rectangular void (Figure 3-4b) are shown, respective before and after filtering. Only 18 coefficients corresponding to the 9 lowest frequencies of total 100 coefficients have been left in the spectrum after filtering ($L = 18$; $N = 100$).

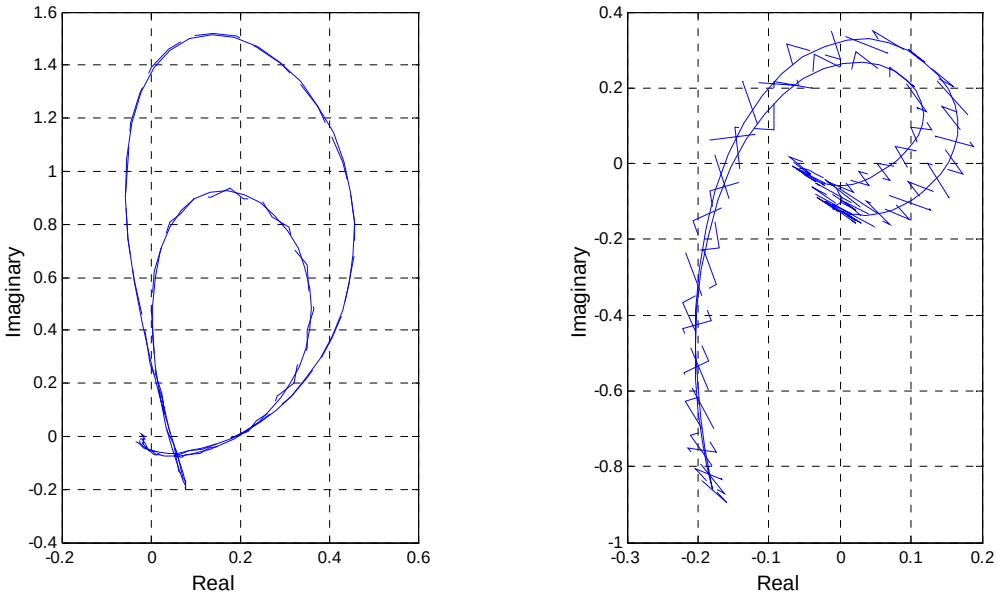

(a) (b)

Figure 3-4. *Vertical lines of the 2D responses presented in Figure 3-2 raw signal (dashed line) and signal after filtering (solid line). Response to a small hole (a) and a notch (b) located 2 mm under surface.*

From Figure 3-4 it can be seen that the proposed filter performs very well, the noise pronounced in the signal presented in Figure 3-4b, introduced by a backlash in the mechanical scanner was efficiently filtered and the shape of the pattern has been well preserved.

4 Results

4.1 Probe comparison

4.1.1 Rohman probe

MDK 33 is a deep penetrating, multi-differential probe developed for aerospace applications. It has a considerable size (square 25 x 25 mm) and a high penetration depth. The probe is build of four different windings forming a cross pattern. The 2D response of this probe is shown in Figure 4-1.

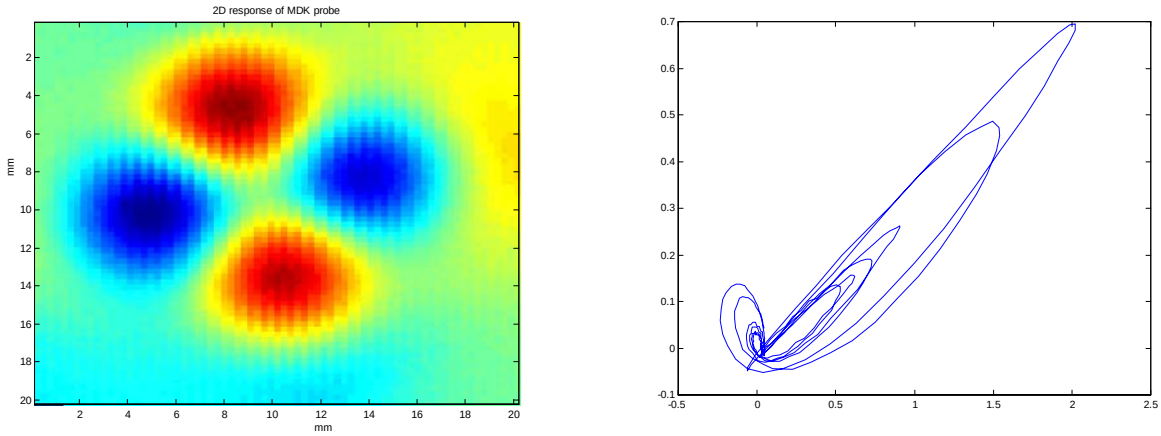

(a) (b)

Figure 4-1. *Responses of the MDK 33. (a) 2D response measured for 1 mm diameter hole at the depth of 2 mm (in-phase component). (b) Responses to 3 holes at the depthh 2 mm.*

4.1.2 Leotest probes

Leotest manufactures a number of MDF probes with different diameters and characteristics. Two types were available in this study: MDF 08 and MDF 12 with diameters respectively 8 and 12 mm. Both probes are similar; they are deep penetrating, multi-differential probes (see /4/ for details).

The probes have different diameters (12 and 8 mm, respectively) and are characterized by a relatively high penetration depth. The probes can be used in the frequency range 200 Hz to 10 kHz. The probes are build of four different windings forming a cross pattern. Since the windings are very well matched very high gains (70–80 dB) can be used without the risc of saturating the instrument, which is essential for low frequencies where pick-ups signals are very low. The 2D response of the MDF 12 probe is shown in Figure 4-2.

Probes' responses to a 2 mm hole at the depth of 2 mm are presented in Figures 4-3 and 4-4 for comparison. The values shown in the impedance plots were obtained for the test frequency 720Hz and gain 76 dB.

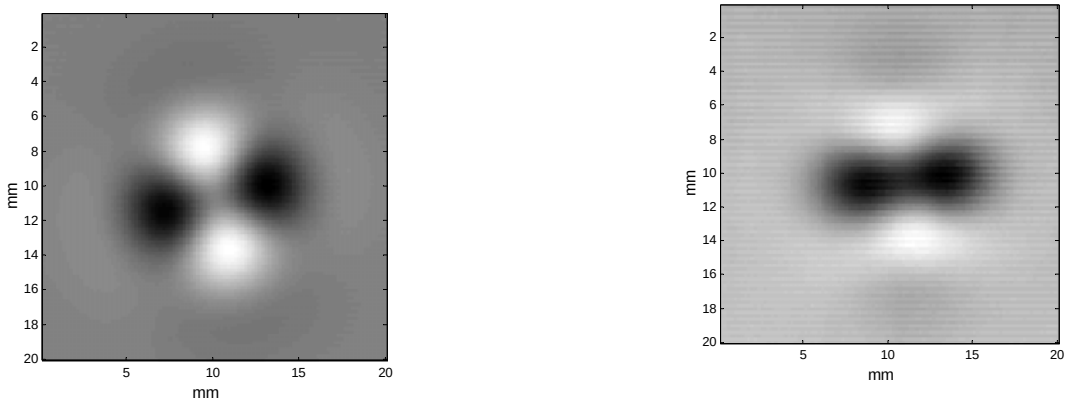

(a) (b)

Figure 4-2. *2D responses of the MDF 12 to a small hole (a), and a rectangular void (b) in a copper plate. Both voids were detected at the depth of 2 mm. An imaginary component of the EC signal is presented in the images.*

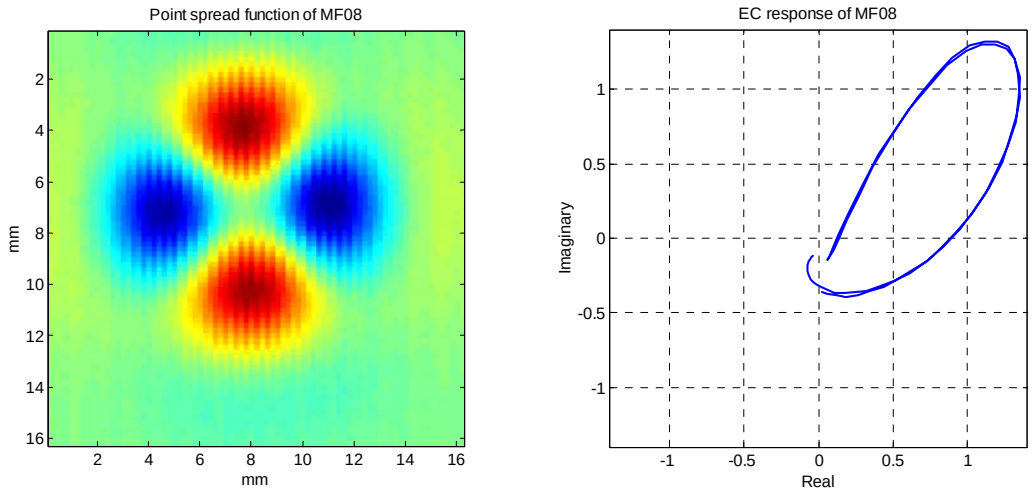

Figure 4-3. *Characteristics of MDF08 probe. PDF shown left and complex response in the middle of probe (vertical scan).*

Probe MDF 08 has approx 6.5 mm between its maximum sensitivity points. The pickups in the multi-differential pairs are symmetrical, which is clearly seen in the complex EC response. Note that the probe's the response can be located in different quarters of the impedance plane depending how on its orientation (cf Figures 4-3 and 4-4).

Active area of the probe MDF 12 is only slightly larger than for the MDF08, the distance between the maximum sensitivity points is approx 7 mm.

Generally, the probes are very similar but the MDF 08 yielded much weaker signals for the deep located voids.

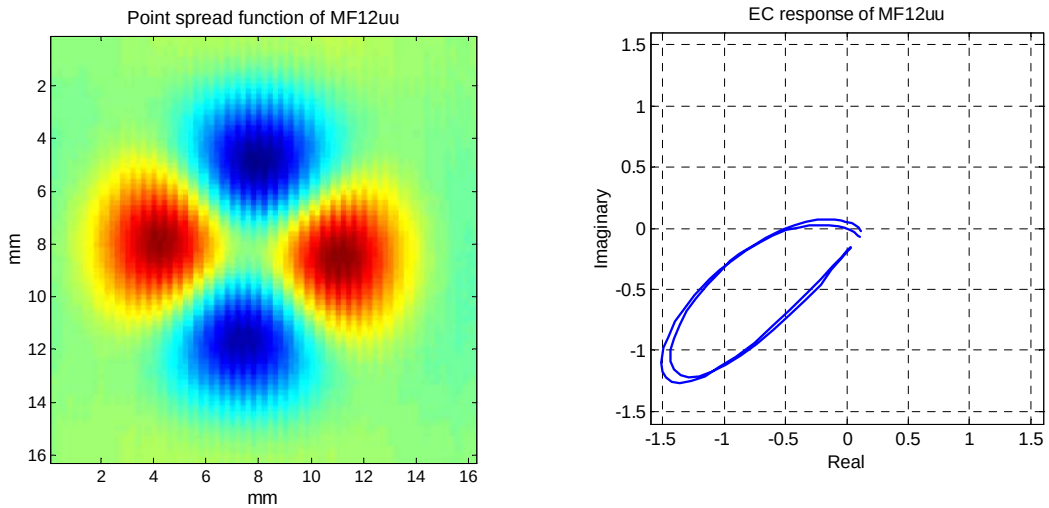

Figure 4-4. *Characteristics of MDF12 probe.*

4.2 Detection limits

Detection limits were established for the probe MDF 12 using cylindrical voids.

The smallest void that could be detected using the probe MDF 12 had diameter of 0.8 mm. The SNR calculated using Equation (2) for this void located at different depths is shown in Figure 4-5. From Figure 4-5 can be seen that the smallest void can be detected at the depths of 4 mm with SNR approx 5 dB and that the void height did not affect the SNR.

SNR estimated for other void diameters and heights are shown in Figure 4-6. It is apparent that the SNR increases for larger diameters and smaller depths. The results obtained for the depths of 1 mm are biased due to the fact that the 1 mm plate had different conductivity than that of the other plates.

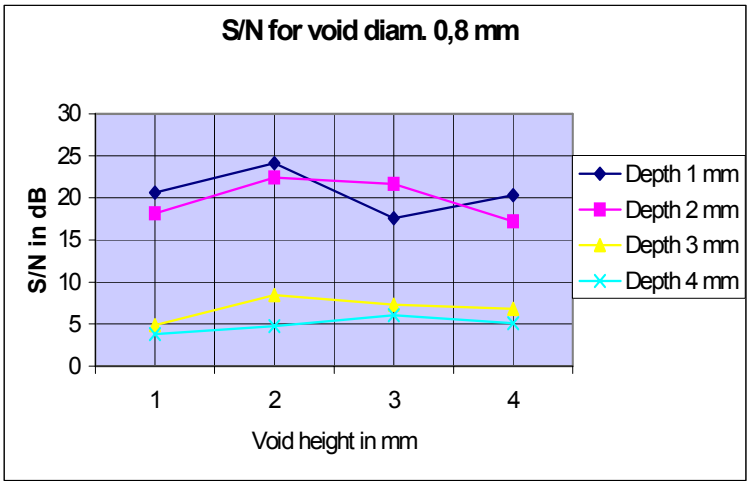

Figure 4-5. *SNR for probe MDF 12 as a function of the void height.*

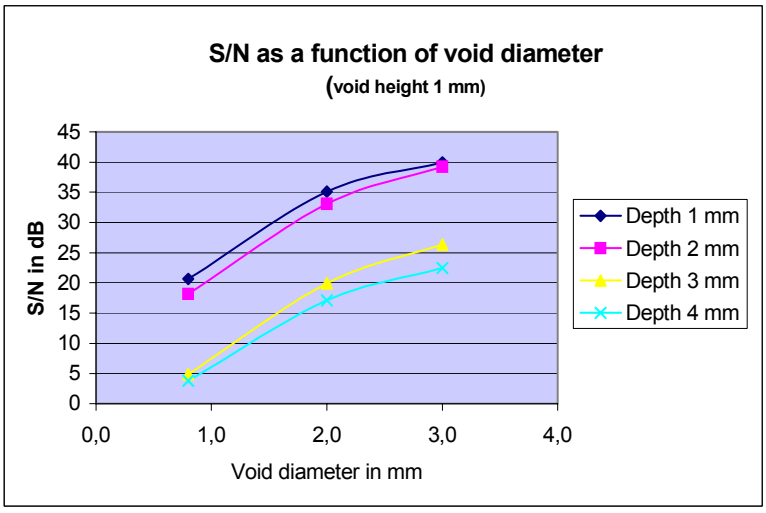

Figure 4-6. *SNR for probe MDF 12 in function of hole diameter.*

4.3 Circular voids

Defect characterization in eddy current is performed using pahse and magnitude of the response. Phase measured in function of the void depth was almost linear (see Figure 4-7), which agrees with the theory. Phase angle decreased with approx 40° per mm.

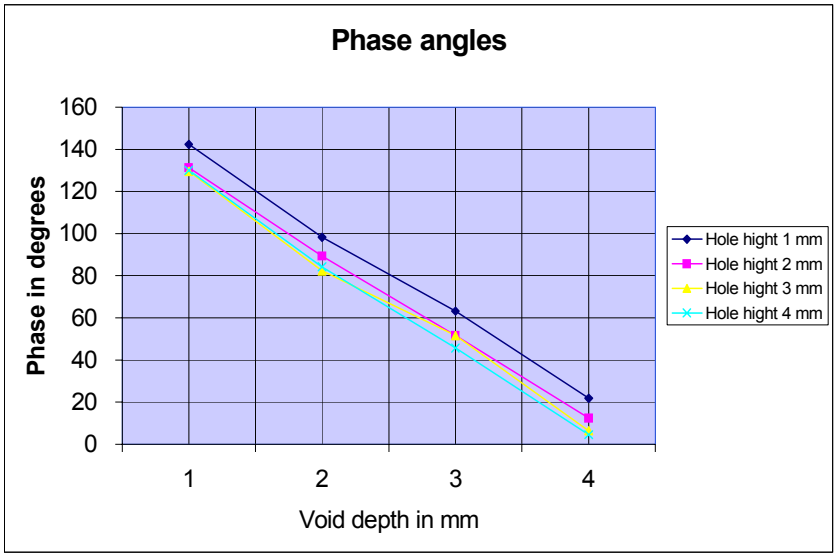

Figure 4-7. *Phase angle for Probe MDF 12 as a function of void depth* t_d.

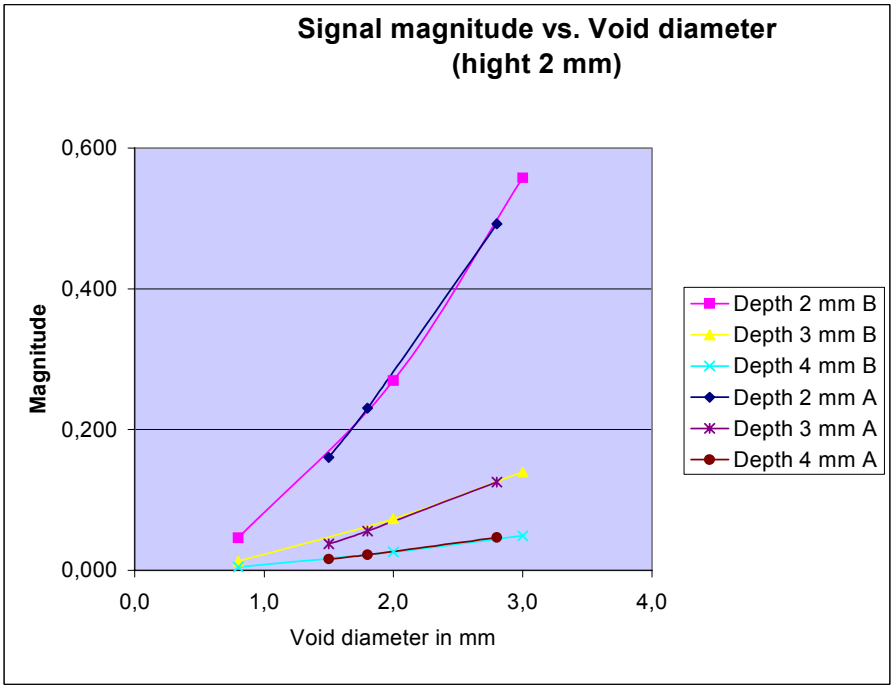

Figure 4-8. *Signal magnitude for Probe MDF 12 as a function of void diameter.*

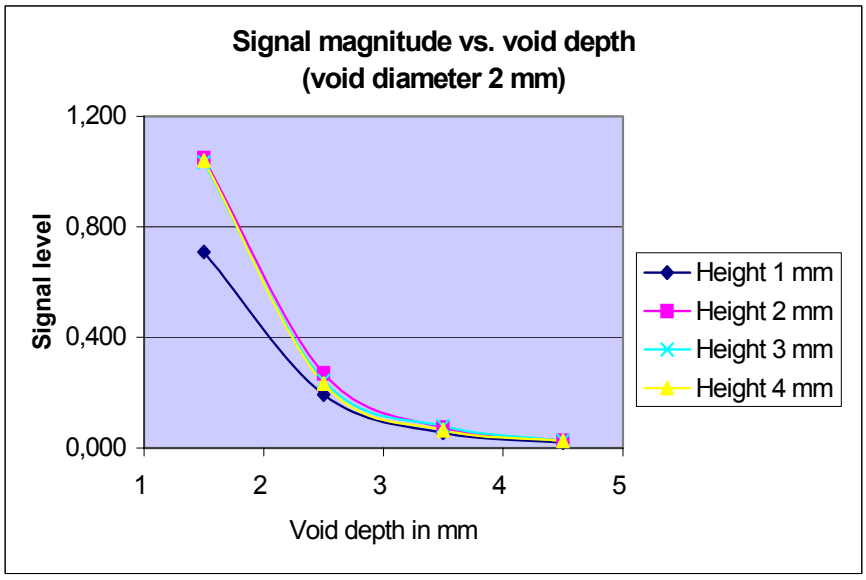

Figure 4-9. *Signal magnitude for Probe MDF 12 as a function of void depths.*

According to the theory signal magnitude should decrease exponentially with void depth, which is apparent from Figure 4-9. Note that the characteristic obtained for 1 mm plate differs from the others due to the difference in conductivity.

4.4 Rectangular voids

4.4.1 Phase angles

Automatic phase estimation defined in Section 3.3 produced consistent results for all tested combinations of plate thickness. Phase angles obtained for the defects widths 0.3 and 0.6 mm are essentially the same. The largest difference in phase measured for defects at the depths of 2 mm was less than 10°. This difference, measured for the depths 3 mm was larger (especially for the smallest defect 1 x 0.3 mm), which can be explained by the decreased SNR in the EC responses from deep defects.

Slope of the phase angle line was the same as for the circular voids, i.e. approx 40° per mm. It was found, however, that the phase angle for certain defect depths was slightly dependent on the thickness of the defect plate, that is, the phase decreased with approx 10° per 1 mm of the plate thickness. See /2/ for details.

4.4.2 Defect size

Results of response magnitude estimation according to the methods defined in Section 2.1 are presented in Figures 4-10, 4-11 and 4-12 using respectively, maximum magnitudes and standard magnitude deviations. Figures 4-10–4-12 show results obtained for three thickness of the defect plate 1, 2 and 3 mm, respectively.

Automatic signal size estimation produces consistent results for all tested defect combinations. The dependence of the response size on the defect length is very well pronounced.

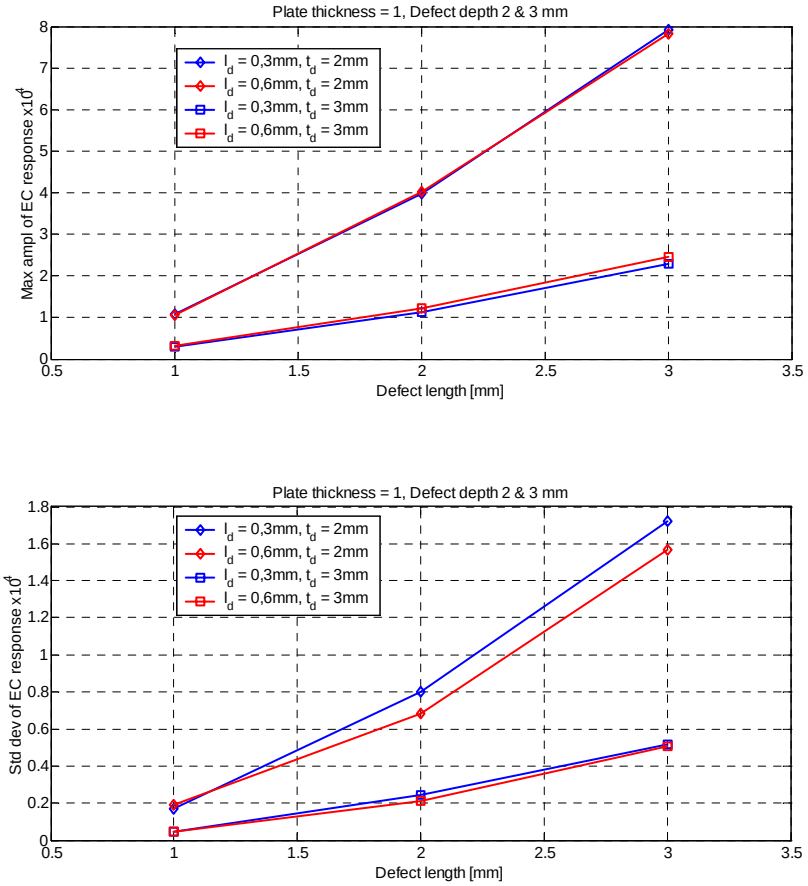

Figure 4-10. *Signal magnitude for Probe MDF 12 as a function of void length and depth (defect plate 3 mm). Manual amplitude measurement (upper), automatic calculation of standard deviation (lower).*

From Figures 4-10–4-11 can be seen that the magnitudes obtained for the plate thickness 2 mm are considerably larger than those for the 1 mm but the corresponding difference between the 2 and 3 mm plates is small.

Interestingly, the response magnitudes obtained for the defects widths 0.3 and 0.6 mm are essentially the same with a tendency for a slightly larger magnitudes for 0.6 mm. This indicates that magnitude the response to the rectangular defect is more strongly related to its lengths than to its area.

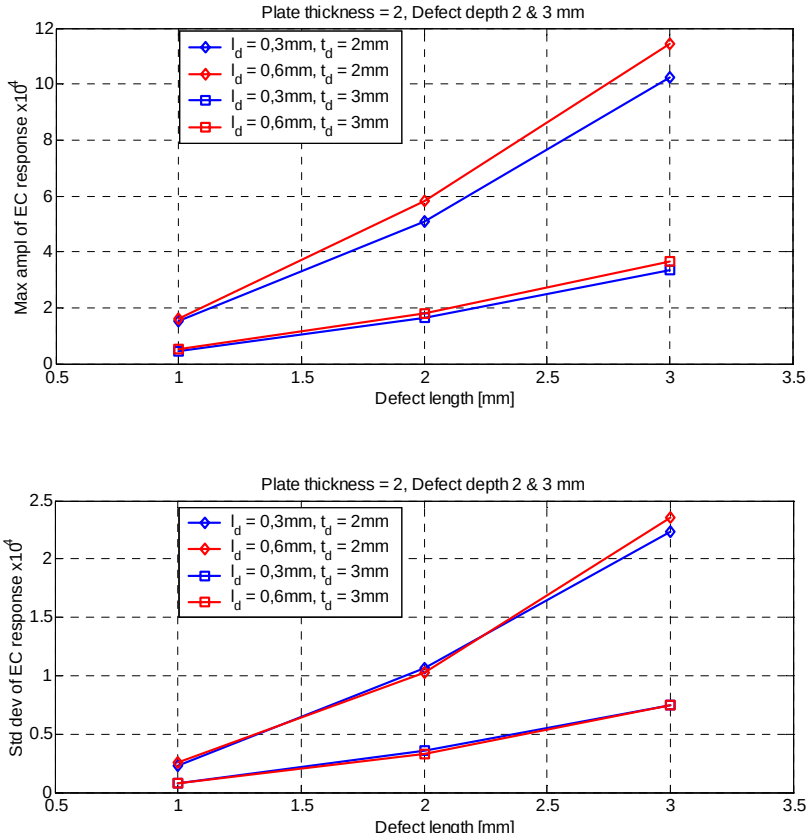

Figure 4-11. *Signal magnitude for Probe MDF 12 as a function of void length and depth (defect plate 3 mm). Manual amplitude measurement (upper), automatic calculation of standard deviation (lower).*

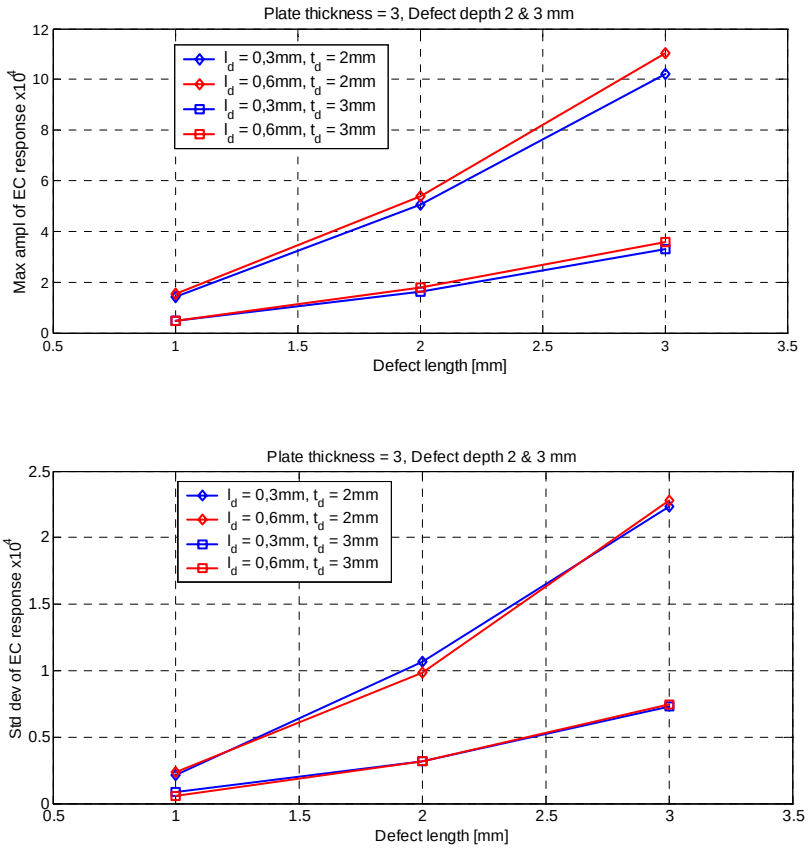

Figure 4-12. *Signal magnitude for Probe MDF 12 as a function of void depths and lengths (defect plate 3 mm). Manual amplitude measurement (upper), automatic calculation of standard deviation (lower).*

4.5 Comparison of EC indications for rectangular and circular defects

4.5.1 Phase angles

Phase angles measured for the circular and rectangular defects are similar if to disregard the 180° difference, which arises from the difference in shapes of the respective responses. The method used for the phase estimation outputs angles in the range of –90° to +90°, that is, it defines the inclination of the eigenvector but not its direction. The direction is assumed based on the location of the points of the EC contour characterized by the maximum magnitude. For instance, if the maximum point is in the first quarter the angle is in the region 0° to +90°, and if it is located in the third quarter the angle is defined between 180° and +270°. This is illustrated by the responses shown in Figure 4-13.

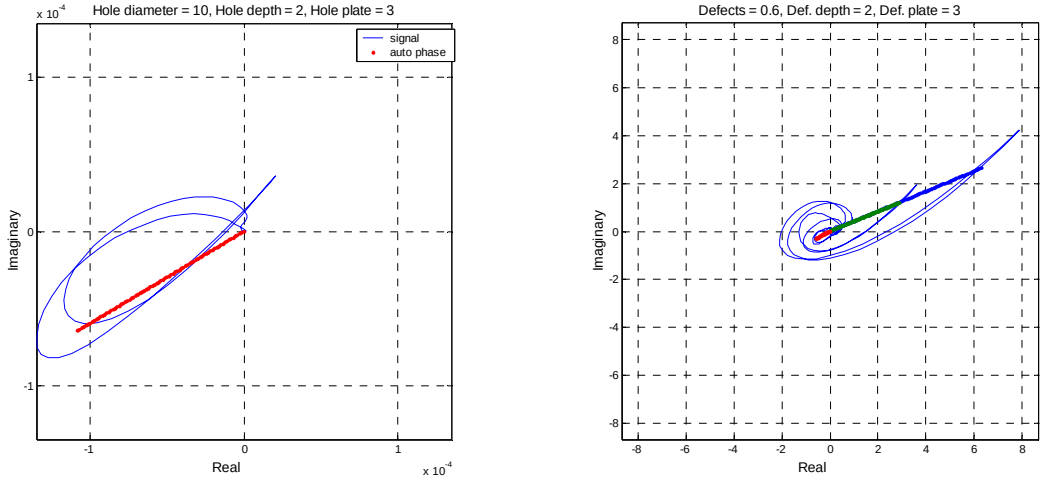

Figure 4-13. *EC patterns for defects at depths 2 mm in plate 3 mm: circular (left) and rectangular (right). Straight lines indicate the estimated phase.*

4.5.2 Defect size estimation

To facilitate the comparison, max magnitudes of the EC responses for circular and rectangular voids are summarized in Tables 4-1 and 4-2 for two different defect depths t_d and two values of defect plate thickness t_v.

Table 4-1. Max magnitudes of the EC responses to the rectangular voids.

Max magnitude of rectangular defects x 10^4					
Defect width 0,3 mm		*td = 2mm*		*td = 3mm*	
Length	*Area*	*tv=2mm*	*tv=3mm*	*tv=2mm*	*tv=3mm*
1	0,3	1,528	1,421	0,442	0,478
2	0,6	5,087	5,065	1,66	1,617
3	0,9	10,241	10,235	3,366	3,295
Defect width 0,6 mm		*td = 2mm*		*td = 3mm*	
Length	*Area*	*tv=2mm*	*tv=3mm*	*tv=2mm*	*tv=3mm*
1	0,6	1,624	1,536	0,526	0,489
2	1,2	5,826	5,372	1,817	1,767
3	1,8	11,439	11,022	3,647	3,580

Table 4-2. Max magnitudes of the EC responses to the circular voids.

Max magnitude of circular defects x 10^4					
		td = 2mm		*td = 3mm*	
Diameter	*Area*	*tv=2mm*	*tv=3mm*	*tv=2mm*	*tv=3mm*
0,8	0,5	1,335	1,825	0,423	0,551
1	0,8	1,865	2,563	0,565	0,776
1,2	1,1	1,901	2,593	0,534	0,742
1,5	1,8	1,855	2,509	0,561	0,779
2,2	3,8	7,222	7,491	2,731	2,371
2,5	4,9	9,012	9,140	3,330	3,055
2,8	6,2	12,804	11,450	3,702	3,831
3,0	7,1	14,744	12,918	4,306	4,531
3,5	9,6	19,244	17,238	5,142	5,412
4,0	12,6	23,211	21,062	6,332	6,742

From the analysis of the above tables it can be seen that the similar magnitudes of the EC responses for circular and rectangular voids occur rather for similar diameters and defect lengths, respectively, than for similar defects cross sections. The diagrams shown in Figure 4-14 illustrate this correlation graphically.

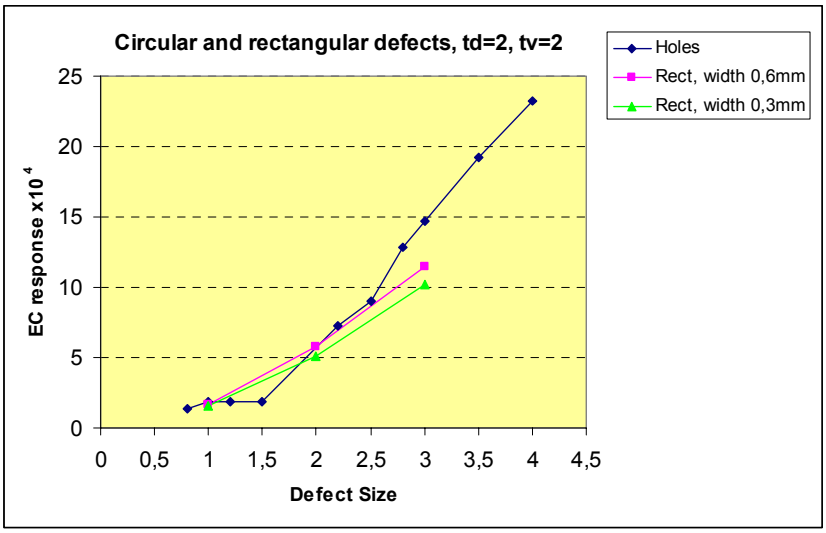

(a)

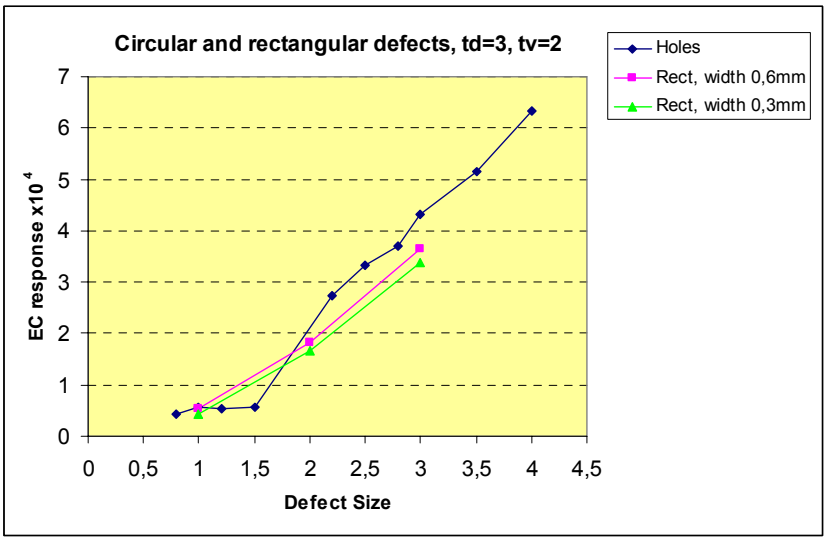

(b)

Figure 4-14. *Magnitudes of the void responses plotted vs their size (hole diameter and rectangular defect length, respectively).*

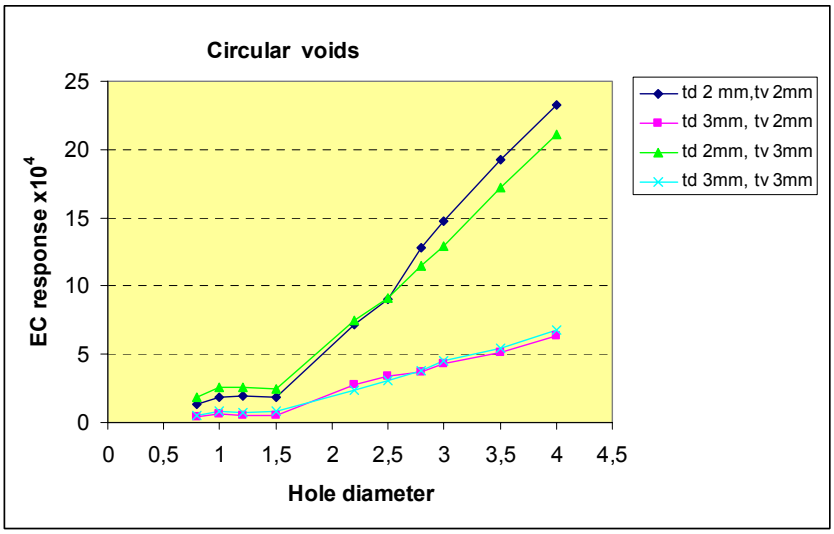

Figure 4-15. *Magnitudes of the circular void responses plotted vs their diameter.*

Magnitude of the response to rectangular voids seems to depend linearly on the void length (in the investigated interval), while for the circular void the corresponding dependence is nonlinear, see Figure 4-15.

4.5.3 Shapes of the EC patterns

The MDF probes are unsymmetrical, which means that, generally, the shape of the EC pattern seen in the impedance plane (at the instrument screen) depends both on the scanning direction with respect to the defect and on the probe orientation. Best results are obtained for the probe orientation 0° or 90°, i.e. for scanning direction parallel to one arm of the cross built up by the probe pick-ups.

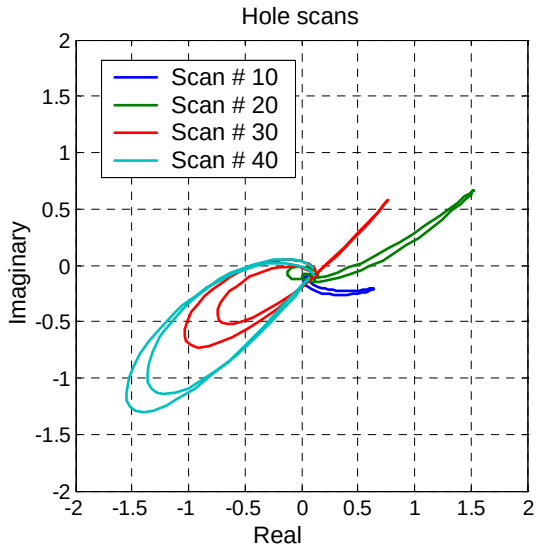

Figure 4-16. *EC responses of the circular void plotted for different scan lines (distance between 10 scans is 5 mm, cf Figure 4-4).*

Since the circular voids are symmetrical the EC pattern obtained using this type of probe will not depend on the scanning direction but only on the probe's orientation with respect to the scanning direction. Examples of complex valued EC patterns obtained for cylindrical voids are presented in Figure 4-16 while Figure 4-17a shows its 2D response.

The 2D responses to rectangular voids are unsymmetrical (see Figure 4-17) and therefore the patterns observed at the screen of the EC instrument take the forms depending on the scan direction. This is illustrated in Figure 4-18 where the EC patterns obtained for vertical (along the void lengths) and horizontal (across the void widths) scanning direction are shown in Figure 4-18a and b, respectively.

Since the defects in the EB weld tend to be located horizontally we decided to use the signal obtained from the scans along the defect lengths (presented in Figure 4-18a) for defect characterization.

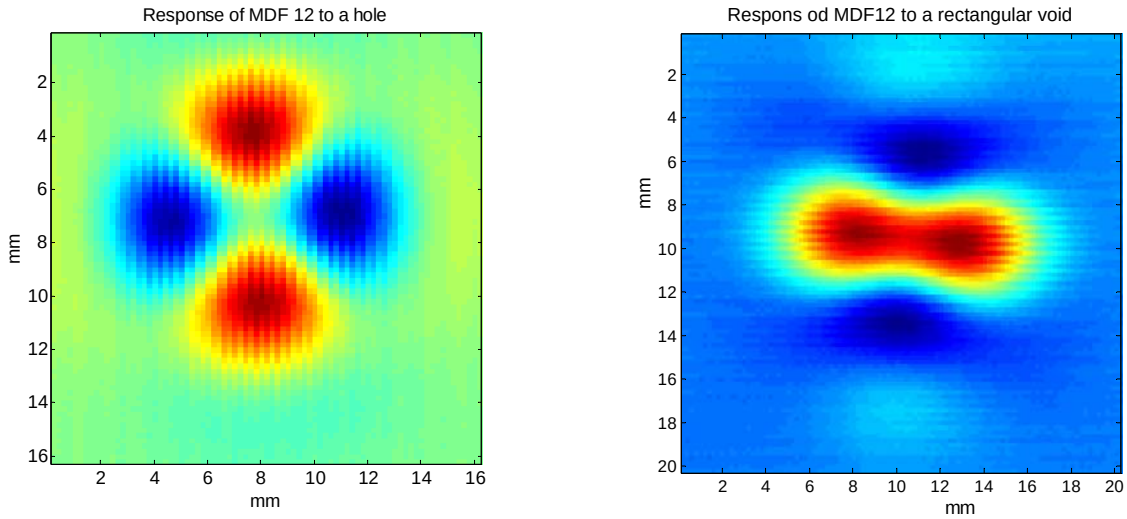

Figure 4-17. *2D responses of the probe MDF 12 to a hole (left) and a rectangular void (right).*

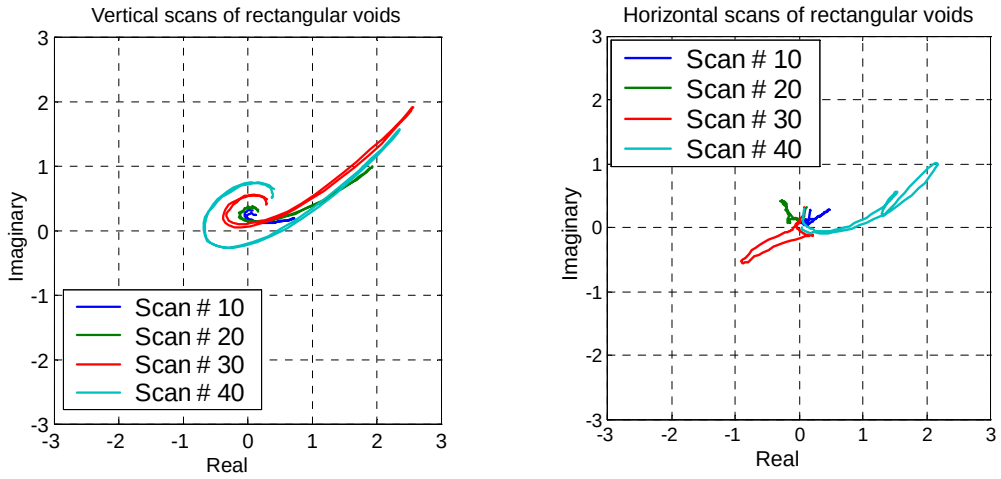

(a) (b)

Figure 4-18. *complex valued responses of the rectangular void plotted for different scan lines (distance between 10 scans is 5 mm, cf Figure 4-17).*

In summary, the MDF12 probes result in asymmetric EC responses to asymmetric defects (e.g. rectangular voids), this means that the EC responses of such defects take different forms depending on the direction of scanning. The phase angles, however, do not change with the scan direction (see Figure 4-18).

5 Comparison of copper material

Four specimens (blocks) from various parts of canister were manufactured to investigate the influence of the copper structure on the EC signals form standard artificial flaws. The flaws in the form of three flat-bottom holes with diameter 2 mm were drilled in each specimen. The hole bottoms were located at the distance respectively, 1, 2 and 3 mm from the upper surface (see Appendix 2 for details). Origin of the four investigated specimens is listed in Table 5-1, all blocks had an identical geometry shown in Figure 5-1. The EC responses for the holes drilled in the Cu blocks were acquired using the MDF12 probe.

Table 5-1. Origin of the test blocks.

Specimen number	Description
1	EBW welding
3	Canister lock
4	FSW weld
5	Canister wall (tube)

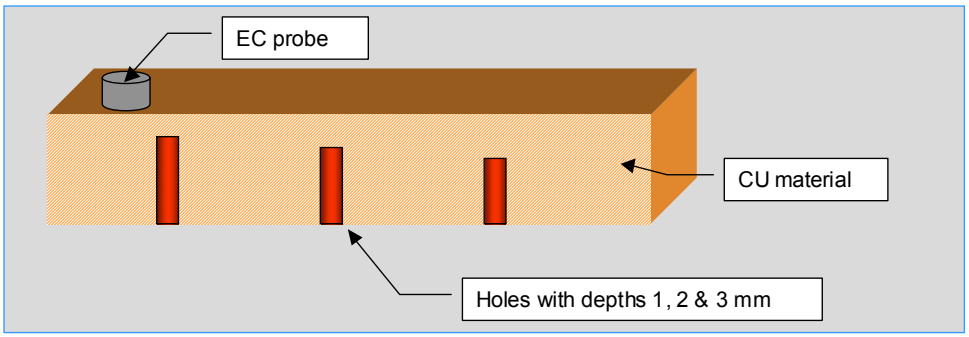

Figure 5-1. *Setup used for comparison of copper blocks.*

5.1 Phase angles

Phase angles of the EC responses acquired from the specimens are listed in Table 5-2. To test the automatic phase estimation described in Section 3.3 the results of manual phase estimation are presented for comparison.

It can be seen that there is no essential difference in phase for different blocks. Average value of the phase obtained for the inspected blocks is plotted in Figure 5-2.

The average slope of the phase line is approx –37 °/mm.

Table 5-2. Phase estimations for four copper blocks specified in Table 5-1.

Probe MDF 12	Phase man			Phase Aut		
Block #	Flaw 1 mm	Flaw 2 mm	Flaw 3 mm	Flaw 1 mm	Flaw 2 mm	Flaw 3 mm
1	86,1	52,5	17,2	84,8	48,1	5,5
3	89,0	54,0	16,4	87,0	51,0	13,0
4	88,6	47,6	15,0	86,6	45,9	6,8
5	86,5	48,6	11,8	83,0	38,6	1,1
Avrage	***87,6***	***50,7***	***15,1***	***85,3***	***45,9***	***6,6***
Std dev	*1,5*	*3,1*	*2,4*	*1,9*	*5,3*	*4,9*

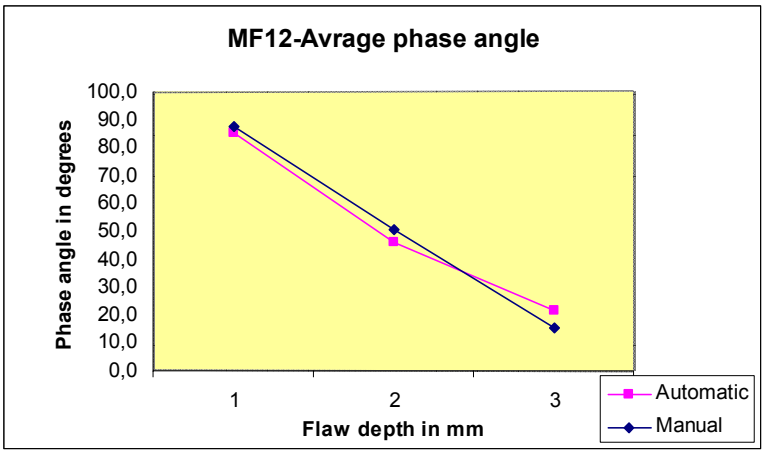

Figure 5-2. *Average phase angles for probe MDF12.*

5.2 Response magnitudes

Magnitudes of the EC responses acquired from the copper specimens are listed in Table 5-3. Two ways of amplitude estimation, explained in Section 3.1 are presented for comparison.

From Table 5-3 and the bar graphs shown in Figure 5-3 it can be seen that there is no essential difference between the blocks. However, the magnitudes obtained for the block # 1 (EBW) seem to be slightly lower than the other values.

Table 5-3. Magnitudes of the hole responses obtained from the copper blocks.

Probe MDF 12						
	Amplitude Abs			Amplitude Std		
Block #	Flaw 1 mm	Flaw 2 mm	Flaw 3 mm	Flaw 1 mm	Flaw 2 mm	Flaw 3 mm
1	1,32E-03	4,21E-04	1,43E-04	4,26E-04	1,43E-04	4,43E-05
3	1,50E-03	4,96E-04	1,75E-04	4,90E-04	1,59E-04	4,98E-05
4	1,61E-03	4,91E-04	1,69E-04	5,43E-04	1,63E-04	5,10E-05
5	1,61E-03	5,40E-04	2,05E-04	4,88E-04	1,62E-04	5,92E-05
Avrage	***1,51E-03***	***4,87E-04***	***1,73E-04***	***4,86E-04***	***1,57E-04***	***5,11E-05***
Std dev	*1,39E-04*	*4,93E-05*	*2,57E-05*	*4,79E-05*	*9,28E-06*	*6,14E-06*

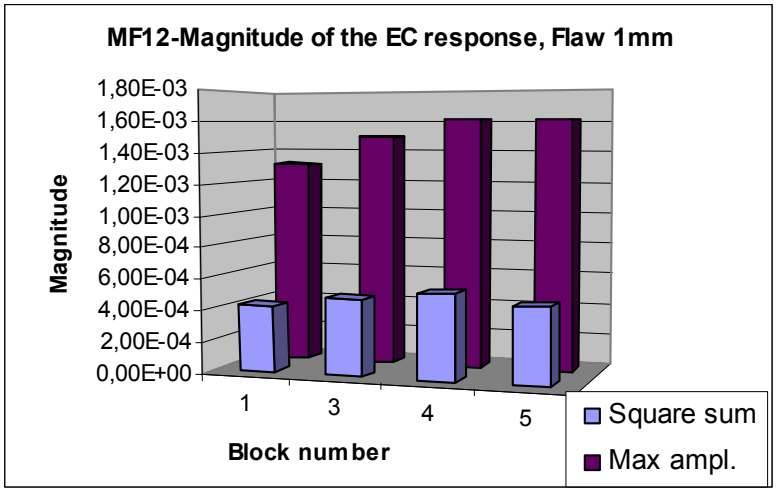

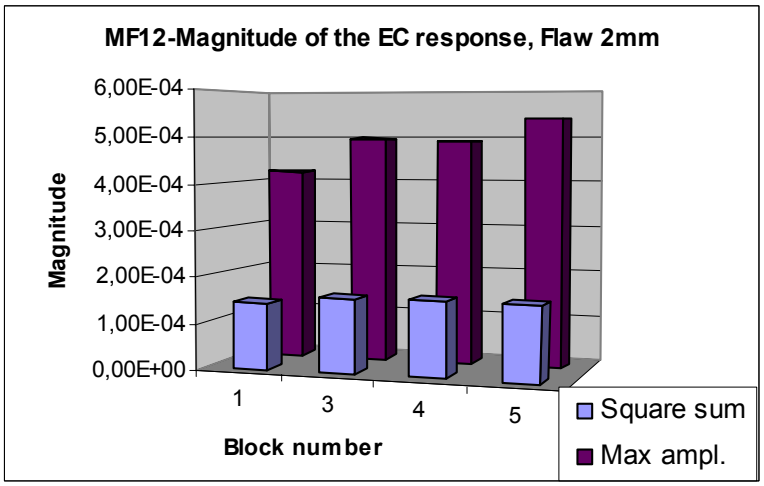

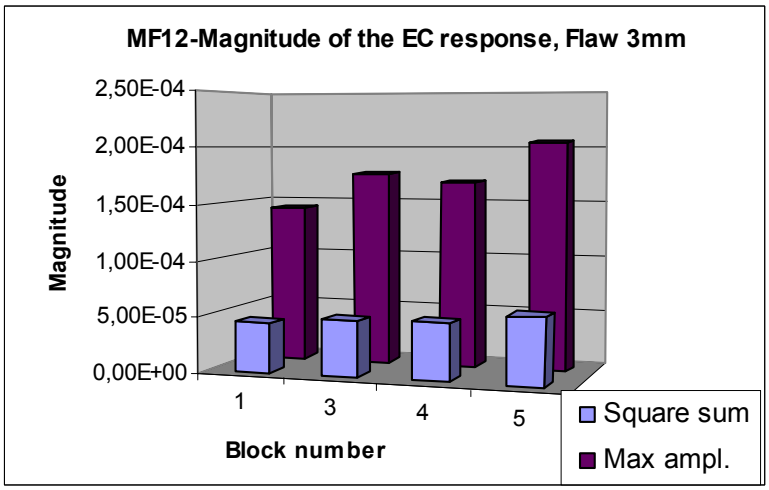

Figure 5-3. *Signal magnitudes from different blocks for probe MDF12.*

Average response magnitude, plotted in Figure 5-4 in logarithmic scale is linear vs hole depth, witch agrees with the theory.

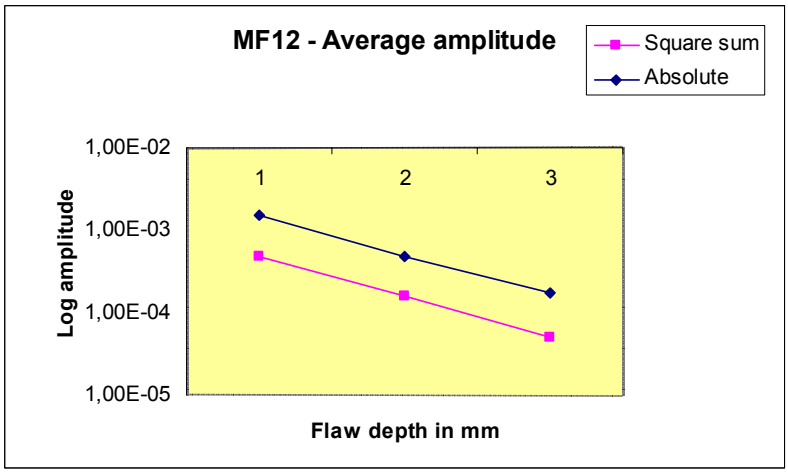

Figure 5-4. *Average magnitudes for probe MDF12 (logarithmic scale).*

6 Conclusions

Comparison of the EC responses to circular and rectangular voids obtained using the MDF12 probe has shown that both types of voids can be characterized using phase and amplitude of their responses in the complex impedance plane.

Phase of the response in the impedance plane appeared to be a reliable measure of void depth. Phase dependence on the void depth is linear (which agrees with the theory) and its slope is approx –37 °/mm.

Magnitude of the EC response contains information on the void size provided that the void depth is known. It has been shown that magnitude of the EC responses is correlated to the lengths of the rectangular voids and hole diameter, this is, similar lengths and diameters result in similar response magnitudes.

It should be noted, however, that multi-differential MDF probes generate responses with different shapes for circular and rectangular voids. First, shapes of the MDF probe responses in the impedance plane depend on the probe's orientation with respect to scanning direction. Second, they also depend upon the direction of scanning with respect to the void orientation. The measurements presented in this report were performed for the probe axis aligned along with the scanning direction and, in case of rectangular voids, for scanning direction along the void lengths.

Comparison of the responses obtained from flat bottom holes in copper material taken from different canister parts has not shown any essential differences between the material samples. Conductivity measurement performed using an absolute EC probe did not show any measurable difference between the specimens.

7 References

/1/ **Stepinski T, 2001.** Deep Penetrating Eddy Current for Copper Canister Inspection, Intenal SKB Report.

/2/ **Stepinski T, 2003.** Eddy Current for Copper Canister Inspection, Part II, Rectangular defects, Intenal SKB Report.

/3/ **Stepinski T, 1994.** "Digital Processing of Eddy Current Signals and Images", Proc of the 6th European Conf. on NDT, Nice, October 1994, pp 51–55.

/4/ **Stepinski T, 2002.** "Deep Penetrating Eddy Current for Detecting Voids in Copper", Proc of the 8th European Conference on NDT, Barcelona, Spain, June 17–21, 2002.

/5/ **Stepinski T, 2003.** "Processing Eddy Current Signals for the Detection of Deep Voids in Copper", presented at Review of Progress in Quantitative NDE, July 27 – August 1, 2003, Green Bay, Wisconsin, USA.

Appendix 1

Realistic defects

Study of natural defects carried out in the project Pr2E.011109 indicates the presence of relatively narrow defects located in the horizontal plane in EB weld.

To enable more detailed defect study using ET a number of realistic artificial defects were manufactured using electro discharge method (EDM) in copper plates with thickness of 1, 2 and 3 mm. Geometry of the EDM defects is shown in the table below:

Plate thickness	Defect size (mm)	Defect size (mm)	Defect size (mm)
1 mm	0.3x1.0	0.3x2.0	0.3x3.0
1 mm	0.6x1.0	0.6x2.0	0.6x3.0
2 mm	0.3x1.0	0.3x2.0	0.3x3.0
2 mm	0.6x1.0	0.6x2.0	0.6x3.0
3 mm	0.3x1.0	0.3x2.0	0.3x3.0
3 mm	0.6x1.0	0.6x2.0	0.6x3.0

Comment

Care should be taken to assure that all plates used for defect manufacturing have the same electrical conductivity (conductivity of the 1 mm plates used in the previous stage of this project differed from the conductivity of other plates). Erosion of defects with width 0.3 mm should start from a hole with diameter 0.29 mm.

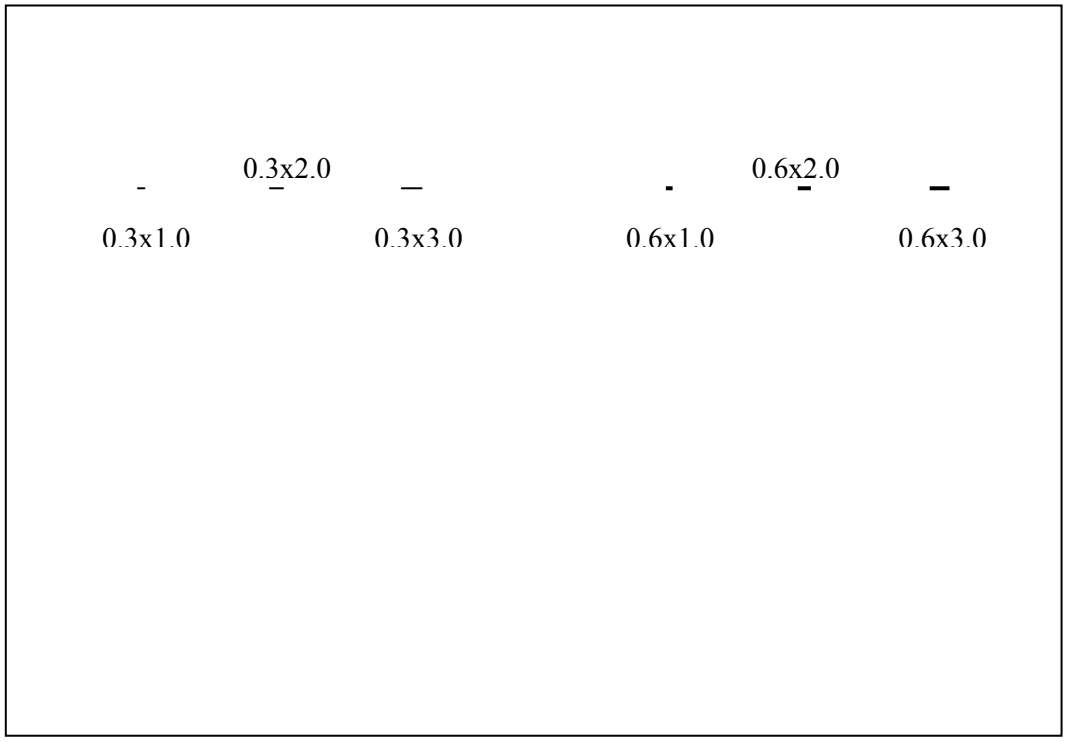

Appendix 2

Influence of material structure

Material samples from lock (sample #3), tube (sample #5), welded material from EBW (sample #1) and FSW (sample #4) were prepared for investigation of the influence of material structure on ET indications. Simple test blocks were manufactured and three flat bottom holes were drilled in each of them. The holes had 2 mm diameter and their bottoms were located respectively 1, 2 and 3 mm from the block upper surface. The samples were taken according to the drawing shown below.

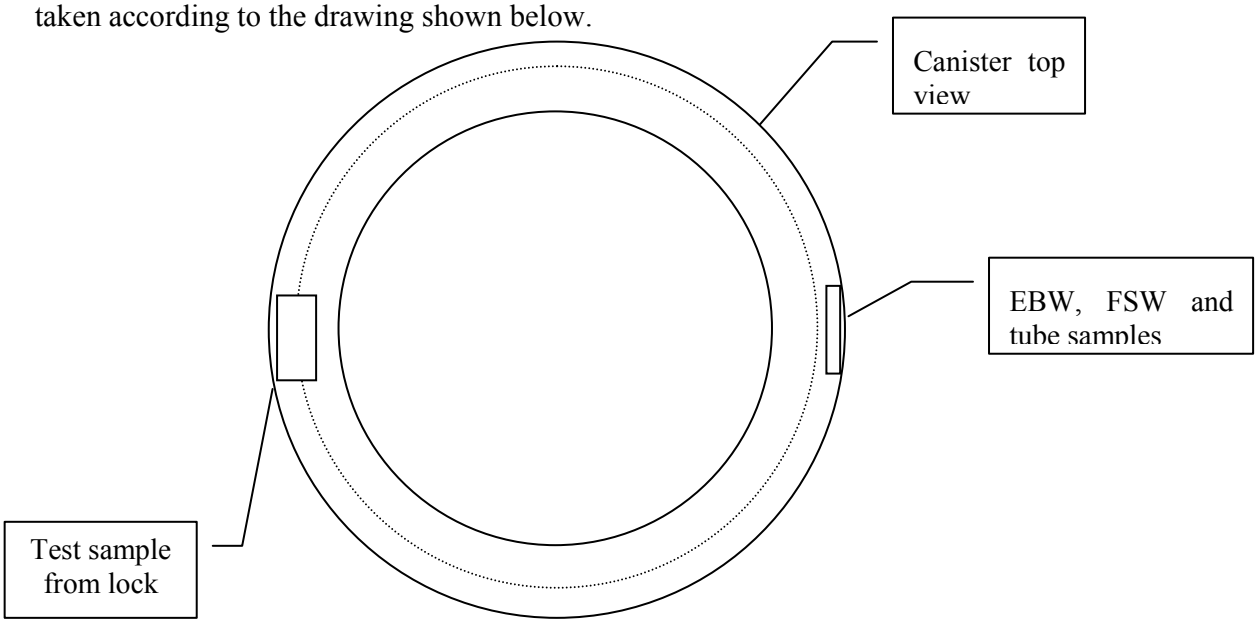

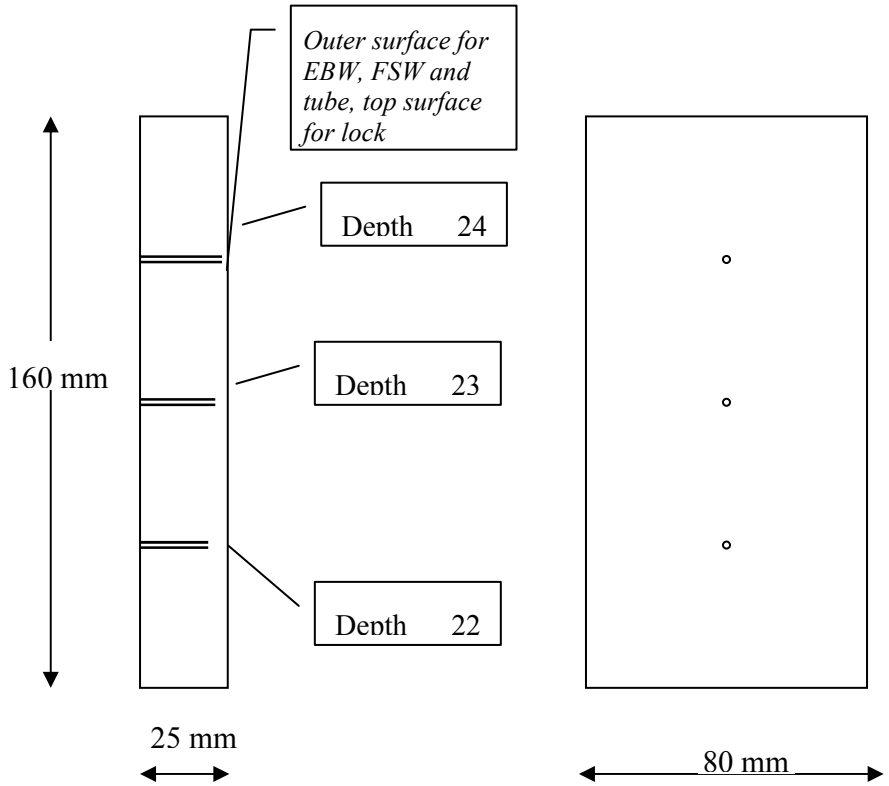

Drawings of sandwich specimen

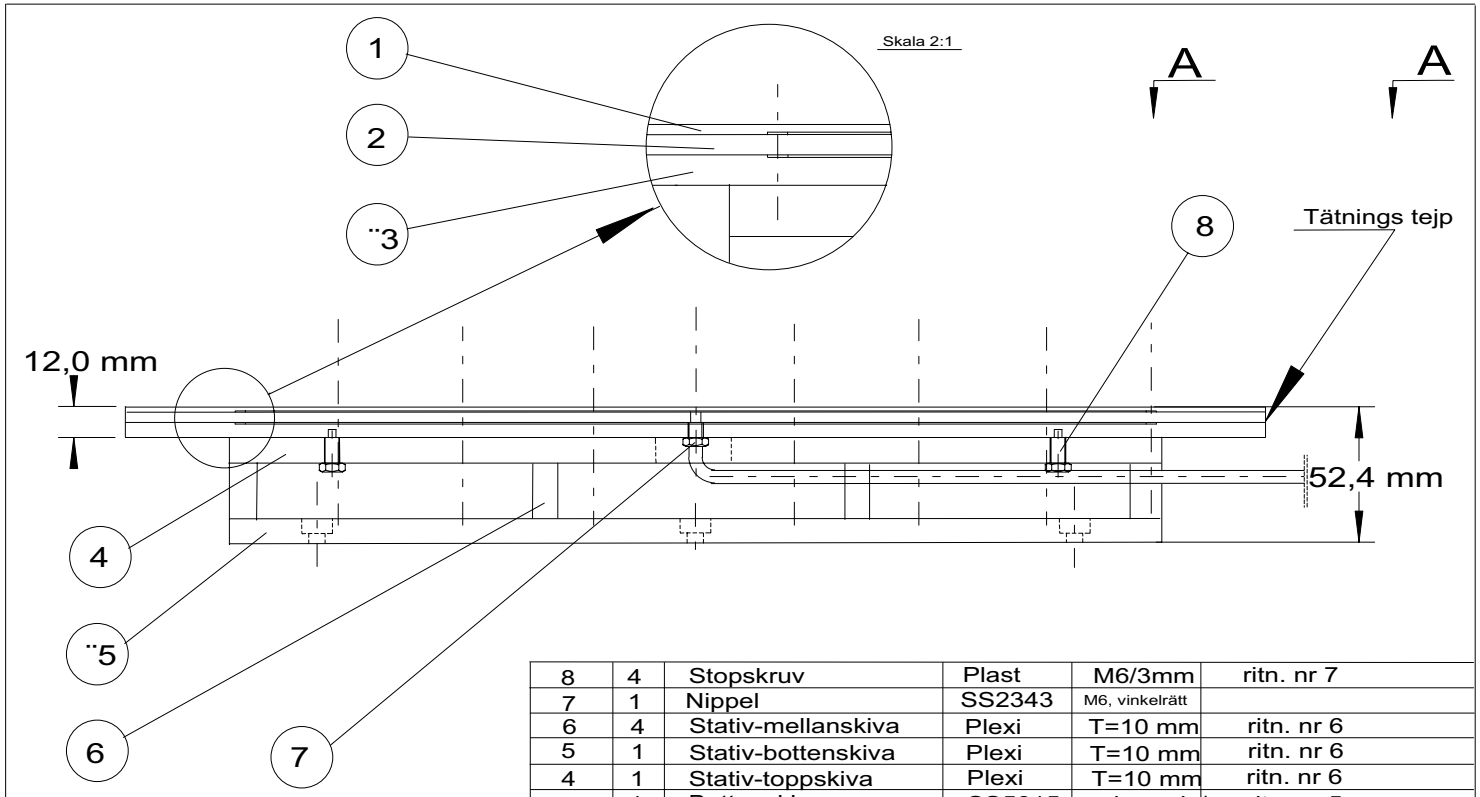

Det.-nr	Ant.	Benämning	Material	Dimension	Anm.
8	4	Stopskruv	Plast	M6/3mm	ritn. nr 7
7	1	Nippel	SS2343	M6, vinkelrätt	
6	4	Stativ-mellanskiva	Plexi	T=10 mm	ritn. nr 6
5	1	Stativ-bottenskiva	Plexi	T=10 mm	ritn. nr 6
4	1	Stativ-toppskiva	Plexi	T=10 mm	ritn. nr 6
3	1	Bottenskiva	SS5015	varierande*	ritn. nr 5
2	1*	Mellanskiva	SS5015	varierande*	ritn. nr 4
1	1*	Toppskiva	SS5015	varierande*	ritn. nr 3

Ritad PW — Skala 1:2 — Art.nr — Dat. 991018

Vy A-A se ritn.2

Signaler och System
UPPSALA, SWEDEN

Plåtstativ-sidovy

Ritn.-nr 1

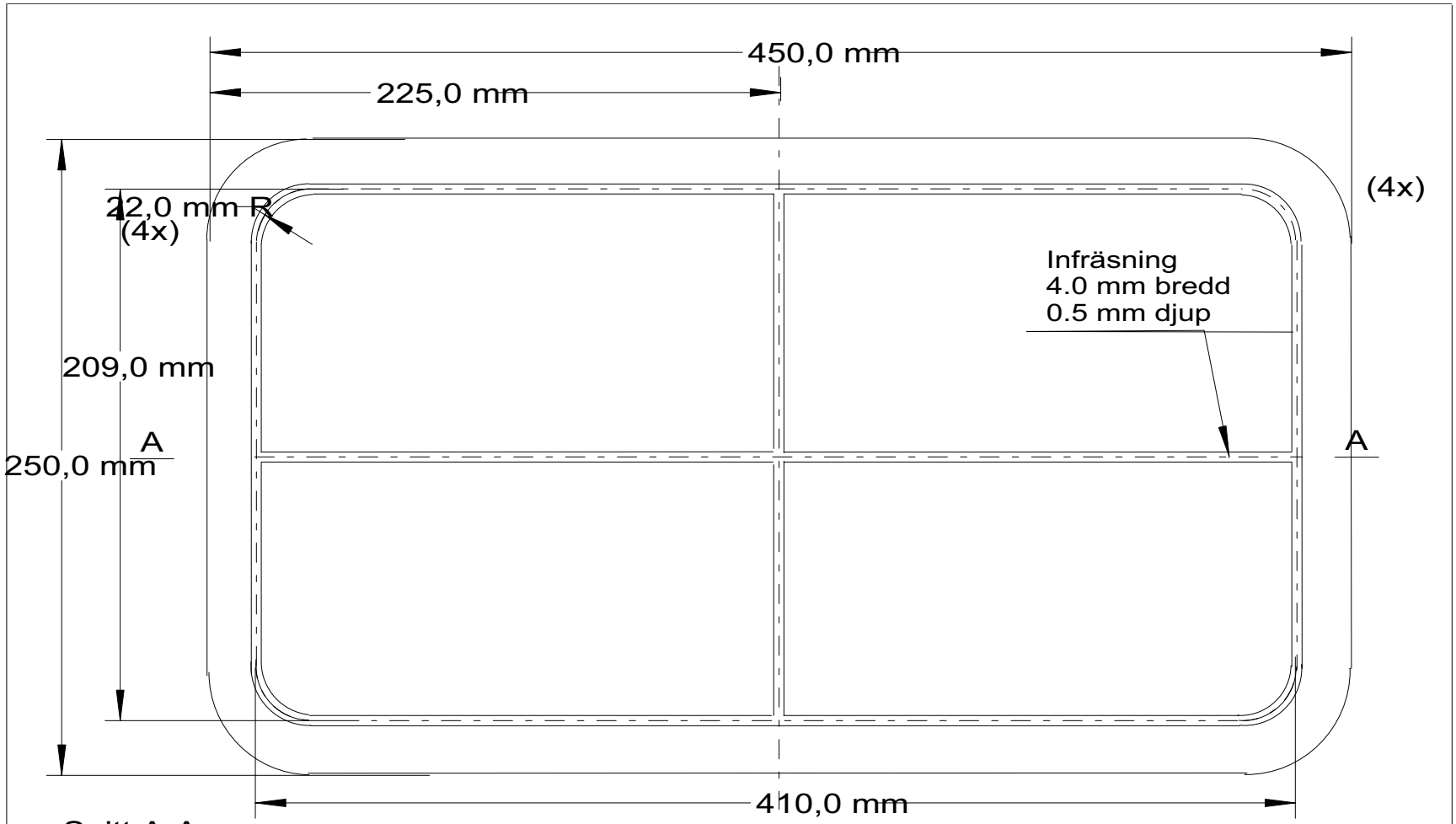

Snitt A-A

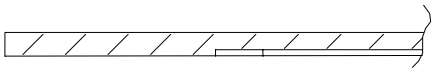

OBS! 4 st plåt med olika tjocklekar 1.0 2.0 3.0 och 4.0 mm.

			SS5015	Tjocklek=	1, 2, 3 och 4 mm		
Det.-nr	Ant.	Benämning	Material	Dimension	Anm.		
	Ritad	PW			Skala 1:2	Art.nr	
Signaler och System UPPSALA, SWEDEN		Toppskiva				Dat.	
						Ritn.-nr	3

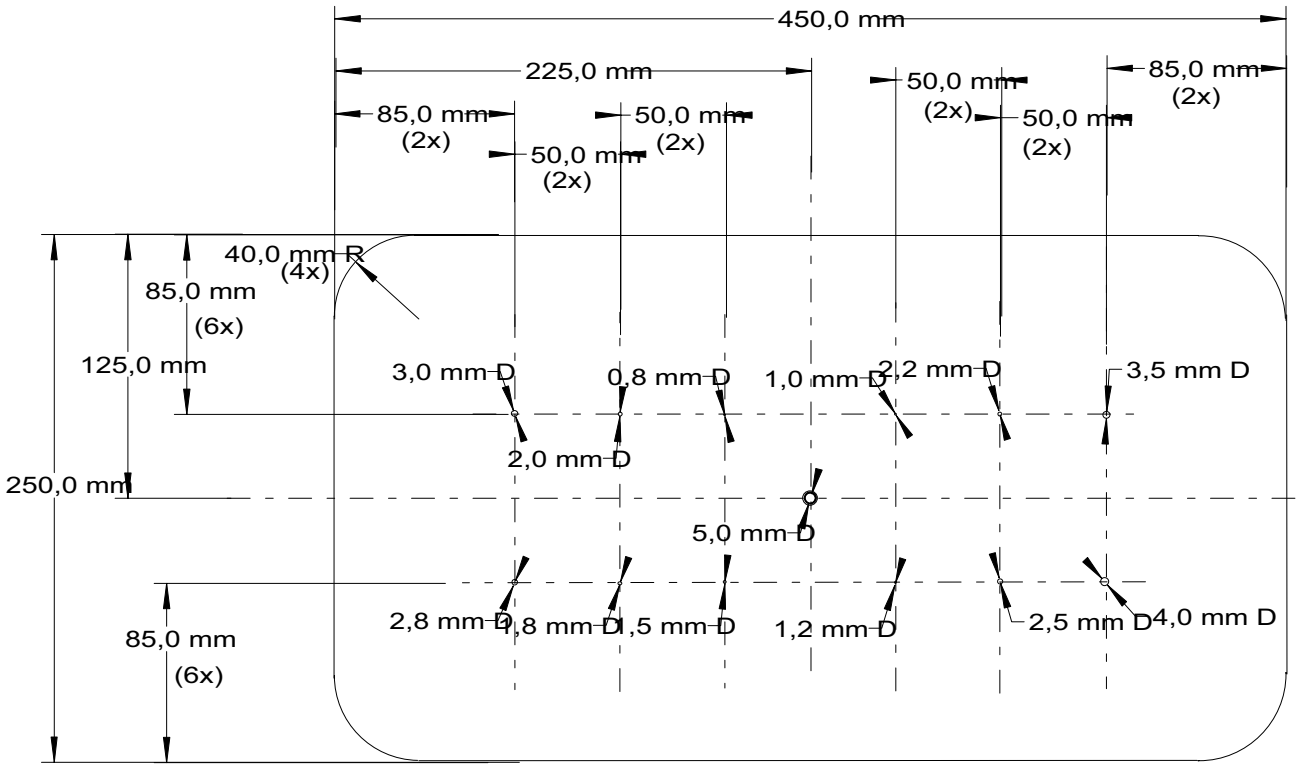

OBS! 4 st plåt med olika tjocklekar 1.0 2.0 3.0 och 4.0 mm.

Det.-nr	Ant.	Benämning	Material	Dimension	Anm.
	Ritad		Skala	1:2	Art.nr
Signaler och System UPPSALA, SWEDEN		Mellanskiva			Dat.
					Ritn.-nr 0-4

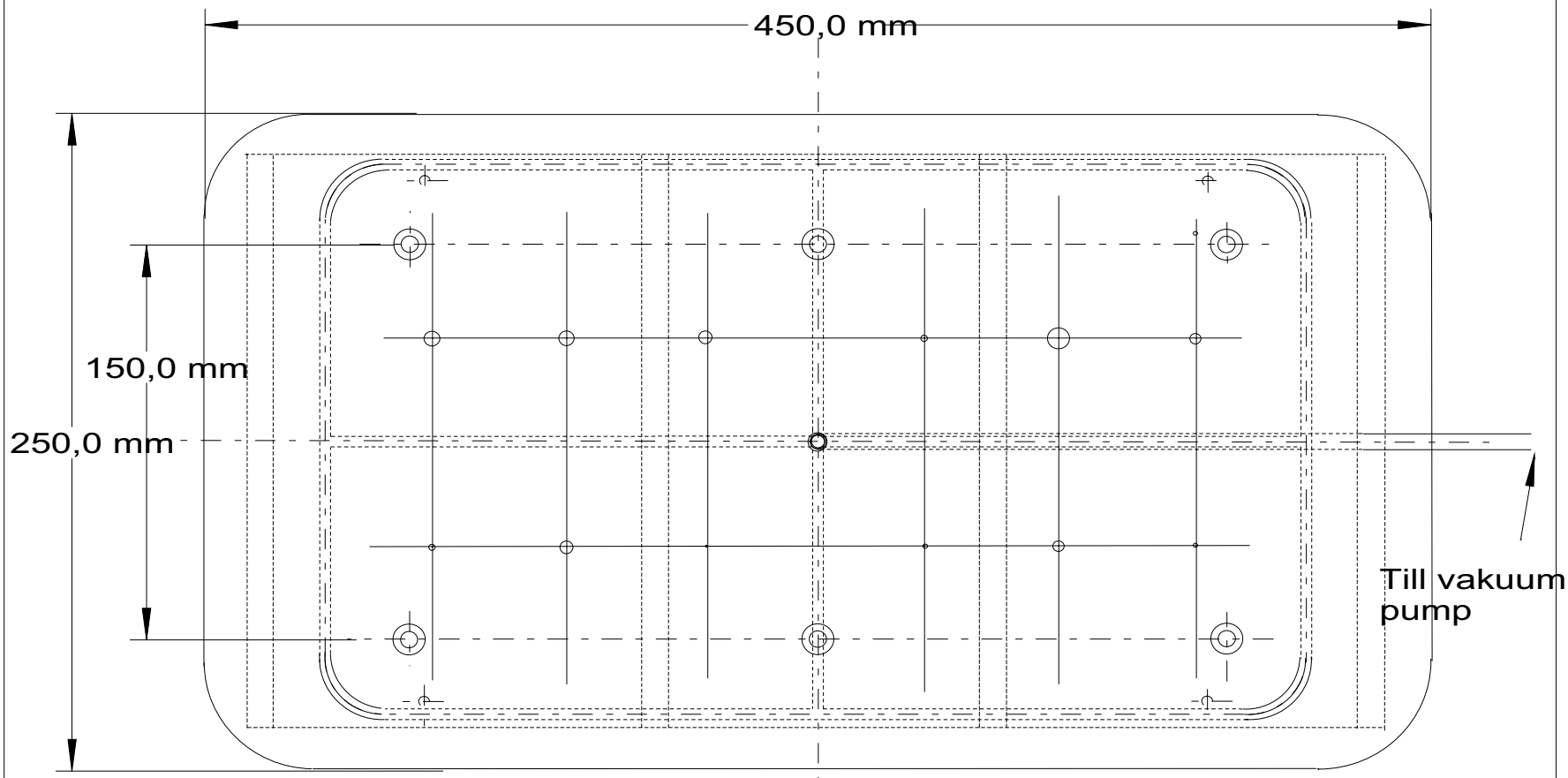

Det.-nr	Ant.	Benämning	Material	Dimension	Anm.
	Ritad PW			Skala 1:2	Art.nr
Signaler och System UPPSALA, SWEDEN		Plåtstativ Vy A-A			Dat. 991018
					Ritn.-nr 2

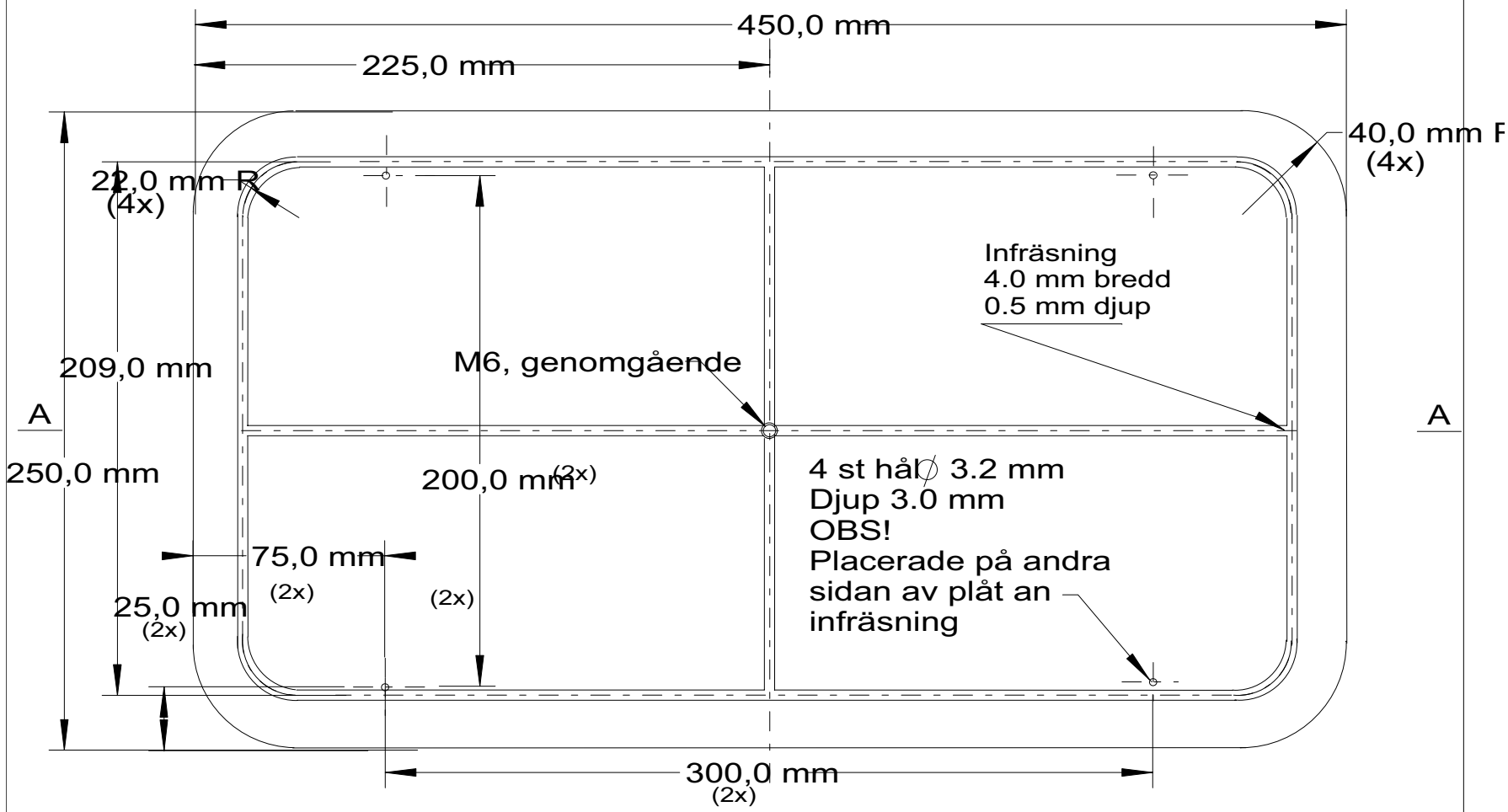

Snitt A-A
Skala 4:1

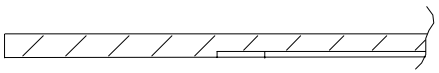

			SS5015	Tjocklek= 6 mm		
Det.-nr	Ant.	Benämning	Material	Dimension	Anm.	
	Ritad	PW		Skala 1:2	Art.nr	
Signaler och system UPPSALA, SWEDEN		Bottenskiva			Dat.	
					Ritn.-nr	5

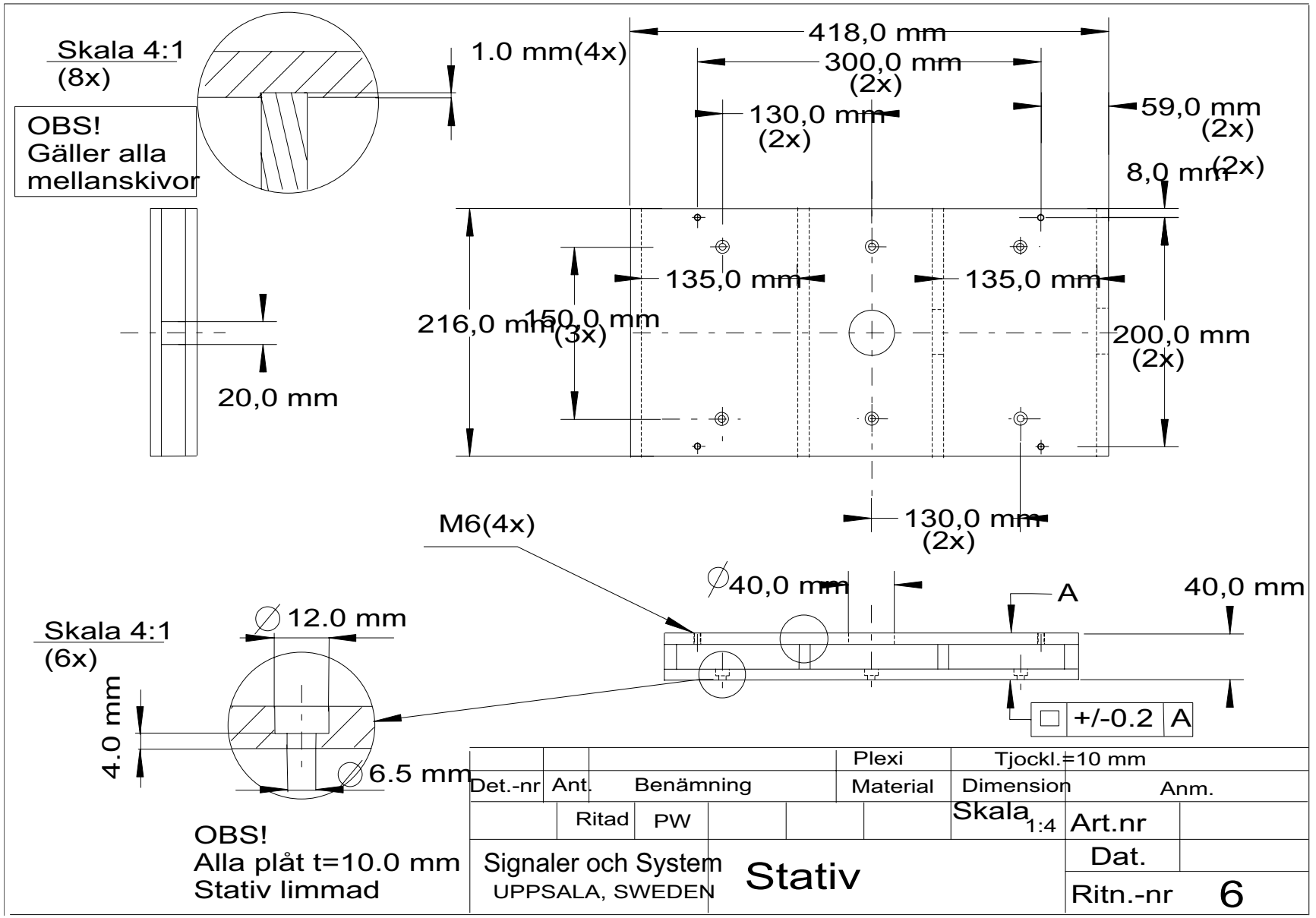
Skala 4:1
(8x)
OBS!
Gäller alla
mellanskivor
1.0 mm(4x)
20,0 mm
418,0 mm
300,0 mm
(2x)
130,0 mm
(2x)
59,0 mm
(2x)
8,0 mm
(2x)
135,0 mm
135,0 mm
216,0 mm
150,0 mm
(3x)
200,0 mm
(2x)
130,0 mm
(2x)
M6(4x)
Ø40,0 mm
A
40,0 mm
Skala 4:1
(6x)
Ø12.0 mm
4.0 mm
Ø6.5 mm
+/-0.2 A
OBS!
Alla plåt t=10.0 mm
Stativ limmad
Plexi
Tjockl.=10 mm
Det.-nr
Ant.
Benämning
Material
Dimension
Anm.
Ritad
PW
Skala 1:4
Art.nr
Dat.
Signaler och System
UPPSALA, SWEDEN
Stativ
Ritn.-nr
6